arXiv:astro-ph/0005463v1 23 May 2000

HST/STIS spectroscopy of the optical outflow from DG Tau: structure and kinematics on sub-arcsecond scales[1]

Francesca Bacciotti[2], Reinhard Mundt[3], Thomas P. Ray[2],
Jochen Eislöffel[4], Josef Solf[4] and Max Camezind[5]

ABSTRACT

We have carried out a spatio-kinematic study of the outflow from the classical T Tauri star DG Tau using the *Space Telescope Imaging Spectrograph* (STIS) on board the Hubble Space Telescope (HST). A series of seven spatially offset long-slit spectra spaced by 0.07″ were obtained along the axis of the outflow to build up a 3-D intensity-velocity "cube" in various forbidden emission lines (FELs) and Hα. Here we present high spatial resolution synthetic line images close to the star in distinct radial velocity intervals (from $\sim$ +50 km s^{-1} to $\sim$ -450 km s^{-1} in four bins, each $\sim$ 125 km s^{-1} wide). The lowest velocity emission is also examined in finer detail (from +60 km s^{-1} to -70 km s^{-1} in five bins $\sim$ 25 km s^{-1} wide). We have found that the highest velocity and most highly collimated component, i.e. the jet, can be traced from DG Tau to a distance D$\sim$0.7″. The jet is on the axis of a pear-shaped limb-brightened bubble which extends between 0.4″ and 1.5″ from the source and which we interpret as a bow shock. Other condensations are seen close to the star indicating ongoing temporal variations in the flow. The low-velocity component of the outflow is found to be spatially wide close to the source ($\sim$0.2″ at D=0.2″), in contrast to the high velocity jet (width $\lesssim$0.1″). We have also found evidence to suggest that not only does the density in the outflow increase longitudinally with proximity to the source but that it also increases laterally towards the flow axis. Thus, at least in the case of DG Tau, the flow becomes gradually denser as it increases in velocity and becomes more collimated. Our observations show a continous bracketing of the higher speed central flow within the lower speed, less collimated, broader flow, down to the lowest velocity scales. This suggests that the low and high velocity FELs in the highly active T Tauri star DG Tau are intimately related. Implications of these observations for FEL models will be considered in a future paper (Bacciotti et al. 2000).

[1]Based on observations made with the NASA/ESA *Hubble Space Telescope*, obtained at the Space Telescope Science Institute, which is operated by the Association of Universities for Research in Astronomy, Inc., under NASA contract NAS5-26555.

[2]School of Cosmic Physics, Dublin Institute for Advanced Studies, 5 Merrion Square, Dublin 2, Ireland.

[3]Max-Planck-Institut für Astronomie, Königstuhl 17, D-69117 Heidelberg, Germany

[4]Thüringer Landessternwarte Tautenburg, Sternwarte 5, D-07778, Tautenburg, Germany

[5]Landessternwarte Königstuhl, D-69117 Heidelberg, Germany

Subject headings: ISM: Herbig-Haro objects — ISM: jets and outflows — star: formation — stars: pre-main sequence

1. Introduction

One of the most interesting questions in young stellar object (YSO) research is how their jets, e.g. Camenzind (1997), Ray (1996) or Eislöffel and Mundt (1997), are collimated and accelerated. To address this problem one must obtain not only high spatial resolution but in addition kinematic information as close as possible to their source. Ground-based long-slit spectroscopic studies of optically visible jet sources have shown that the structure and kinematics of the outflow region on scales $\lesssim 1''$ is rather complex (e.g. Solf and Böhm (1993); Hirth, Mundt, and Solf (1997)). In a significant fraction of classical T Tauri stars (CTTSs) the forbidden emission lines (FELs) show two (or more) blueshifted velocity components which have very different properties (note that in many CTTSs the corresponding redshifted part of the flow is occulted by a circumstellar disk, at least close to the source). In the case of double-peaked FEL profiles, the emission consists of a so-called high-velocity component (HVC), having typical radial velocities of -60 to -200 $\mathrm{km\,s^{-1}}$ and a low-velocity component (LVC), having typical radial velocities of -5 to -20 $\mathrm{km\,s^{-1}}$ with respect to the systemic velocity of the star (see Hartigan, Edwards, and Ghandour (1995) and Solf (1997) for comprehensive discussions). While the HVC can be spatially very extended (at least in the outflow direction) and is often identified with a jet, the LVC is much more compact ($\lesssim 1''$). Other differences between the two components have also been noted, for example the LVC appears to be of higher density but lower excitation than the HVC (Hirth, Mundt, and Solf 1997) and the LVC shows a clear inverse correlation of velocity with increasing critical density. The latter effect has been interpreted as evidence of acceleration in the LVC with increasing distance from the star.

A number of theories have been put forward to explain the origin of the various FEL components. For example Kwan and Tademaru (1988, 1995) have suggested that the LVC and HVC are separate flows. According to their model the LVC is a poorly collimated wind coming from the outer periphery of the YSO disk while the HVC is a separate jet launched from closer to the star. Others have sought to explain the observations in terms of a one component, non-isotropic, wind model in which the appearence of separate FEL components is due to projection effects (Hartmann and Raymond 1989; Safier 1993; Ouyed and Pudritz 1994). In any event, Calvet (1997) has shown that the luminosity of the two components is tightly correlated, which seems to imply that they are not independent flows, and that the apparent dominance of one component over the other may be a density effect.

In order to examine in more detail the nature of the compact FEL region, we have observed the CTTS DG Tau with STIS on-board the HST. Multiple overlapping slit positions parallel to the outflow from this star were chosen so as to build up a 3-D spatial intensity-velocity "cube". Our target was picked not only because it is one of the closest CTTSs, but more significantly because its FEL region has a broad range of velocities, probably also a result of the relatively small

angle between the jet axis and the line of sight ($\approx 38°$, see Eislöffel and Mundt (1998)). This is important given the moderate wavelength resolution of STIS. Historically, DG Tau was amongst the first T Tauri stars from which a jet-like outflow (HH 158) was discovered (Mundt and Fried 1983) and it has been imaged by the HST prior to the installation of the telescope's correcting optics (Kepner et al. 1993). On large scales ($\approx 10''$) the jet seems to terminate in a bow shock (Eislöffel and Mundt 1998) while high resolution spectro-imaging ground-based studies (Lavalley et al. 1997) have shown that the flow close to the star contains at least two resolved knots (at $2.7''$ and $4''$, epoch 1994.8). The outermost of these has a morphology and velocity gradient which is also consistent with it being a bow shock.

In §2 we describe our observational technique and give details of our STIS data. Our primary results are described in §3 and discussed in §4. A more detailed analysis will be presented in Bacciotti et al. (2000).

2. Observations

STIS spectra of DG Tau were taken on January 14 1999 using the G750M grating and a central wavelength setting of 6581 Å. The spectral range of 562 Å included several strong forbidden lines ([OI] $\lambda\lambda$6300,6363, [NII] $\lambda\lambda$6548,6583, [SII] $\lambda\lambda$6716,6731) as well as Hα. The STIS/CCD detector, a 1024×1024 pixel array, had a spectral resolution of 0.56 Å pixel^{-1} and a nominal sampling of $0.05''$ pixel^{-1} in the dispersion and spatial directions respectively. The actual spatial resolution, however, was limited by the PSF of the HST in the red to a FWHM of approximately $0.1''$. The slit aperture was 52×0.1 arcsec^2. Seven different long-slit spectra were taken, keeping the slit parallel to the outflow axis (P.A. 226°), but with steps of $0.07''$ in the transverse direction, i.e. with offsets southeast and northwest of the jet axis. In this way we built-up a 3-D flux density/radial velocity data cube of the optical outflow from DG Tau, with a total spatial width of about $0.5''$ in the direction perpendicular to the jet axis. The spectra are labelled S1,S2,...S7 going from the southeast to the north-west; the central slit position (S4) coincided with the star (RA $4^h\ 27^m\ 04^s.71$, Dec $+26°\ 6'\ 16.8''$.) Exposure times were split in order to facilitate removal of cosmic rays. Total exposure times were approximately 2740 s for S1 – S5, 1930 s for S6 and 2050 s for S7. Note that the somewhat shorter exposure times for the last two spectra were due to minor problems with the HST.

The pipeline spectra were found to be contaminated by a large number of "hot" pixels and so the raw data were first fully re-calibrated using the *CALSTIS* suite of programs and new reference files made available by the STScI. Subsequent reduction and data analysis was carried out using standard IRAF routines. In order to minimise contrast problems close to the source, the stellar continuum, and that of a faint reflection nebula extending up to $2''$ from the source, were carefully subtracted from all images. This operation proved to be particularly critical for the central spectra S3, S4, and S5, due to the appearance of artificial undulations in the stellar continuum, caused by sampling effects (see the STIS Handbook v3.0).

From the acquired spectra we created synthetic 2-D images for the various lines in four broad distinct radial velocity intervals (Figs. 1–2). These images were constructed by adjoining the seven row-averaged columns of pixels obtained from S1–S7 for the corresponding velocity bin. Averaging was done over five columns, corresponding to approximately 2.83Å, in the dispersion direction. In order to study the lowest velocity emission in finer detail, we also (Fig. 3) carried out a similar procedure in [OI]λ6300 and [SII]λ6731 but this time using just one column in the dispersion direction. All velocities quoted in this *Letter* are systemic using $v_{\star,hel} \approx +16.5\,km\,s^{-1}$, as derived from the Li λ6707 photospheric absorption line.

3. Results

Our composite images of the outflow close to DG Tau in the four broad velocity bins, and in each of four lines (Hα, [NII]λ6583, [SII]λ6731, and [OI]λ6363), are shown in Figs. 1 and 2. Note that we did not include [OI]λ6300 in these figures as the blueward portion of this line was missing from our spectra due to a restricted choice for the STIS central wavelength. The velocity range is approximately $+50\,km\,s^{-1}$ to -450 $km\,s^{-1}$ and the four velocity bins (low, medium, high, and very high), with widths of about $125\,km\,s^{-1}$, represent increasingly blueshifted velocities. On all figures the position of the star (i.e. the peak in the continuum subtracted light) is marked. Similar images, for the [OI]λ6300 and [SII]λ6731 lines, but only for the lowest velocities (from about $+60\,km\,s^{-1}$ to -70 $km\,s^{-1}$) and with bin widths of only about $25\,km\,s^{-1}$, are shown in Fig. 3.

First of all, we note that the appearence of the outflow changes, remarkably in some cases, from line to line and from velocity bin to velocity bin (see in particular Figs. 1 and 2). The jet from DG Tau is, as one might expect, most evident at the highest velocities and is visible as a narrow feature up to about 0.7″ from the star. We will discuss it in more depth shortly. Aside from the jet a limb-brightened bubble-like structure can also be observed that extends between 0.4″ and 1.5″ from DG Tau. The "bubble", which is most evident at intermediate velocities, in combination with the jet, gives an overall pear-shaped morphology to the emission.

Comparison of Figs. 1, 2 and 3 lead to a number of important results:
(i) The lowest velocity emission close to the star ($\lesssim$0.3″) is spatially broad, i.e. it is well resolved in the transverse direction to the outflow, but it does not extend far along the flow.
(ii) Within $\lesssim$0.5″ from the star, there appears to be a more or less gradual increase in the degree of collimation with velocity: at high and very high velocities, the flow is primarily confined to the central axis.
(iii) Beyond 0.5″ from the star there are at least two well-defined structures (which we have labelled A1 and A2 in the medium velocity Hα image following the knot nomenclature of Eislöffel and Mundt (1998)). The outermost one, A1, is bow-shaped and observed in all lines but the innermost one, A2, is more easily seen in Hα. There is very high velocity gas immediately behind A1, which is seen in all lines but which is not symmetrically distributed around the jet axis. The opposite effect is, incidentally, seen near A2 where the higher velocity gas appears in the *downstream* direction.

The emission from A2 is also distributed asymmetrically with respect to the outflow axis.
(iv) Comparison of the [OI], [SII], and [NII] data (in Figs. 1 and 2) show that the central jet can be traced much closer to the source in [OI] and [NII] than in [SII]. This result is probably due to a combination of quenching and excitation effects (see Bacciotti et al. (2000) for details). Note that the [OI] line has a 100 (10) times higher critical density than the [SII] ([NII]) line, and that the [NII] line usually traces gas of higher excitation. The emission peak (centroid) in the [SII] and [OI] images moves outwards with increasing velocity. This effect is visible at all velocities, but it is most obvious at the highest velocities where virtually no [SII] emission and only faint [OI] emission is seen in the region $\lesssim 1''$. Since the high velocity jet can be traced right back to the source in Hα, the lack of high-velocity and the presence of low-velocity FEL emission at $< 1''$ can probably only be explained by quenching effects in *both* the longitudinal and lateral directions. In other words our data suggest that the jet density increases not only with proximity to the star (in the longitudinal direction) but also transversely toward the outflow axis. Without the latter effect one would not be able to explain why there is so much spatially extended and easily quenchable *low-velocity* FEL emission seen so close to the source.
(v) Quenching effects likewise manifest themselves at low velocities (see Fig. 3) in that the centroid of the low velocity [OI]λ6300 emission is closer to the star than the centroid of the [SII]λ6731 emission. This was expected on the basis of groundbased measurements (Hirth, Mundt, and Solf 1997).
(vi) In the region close to the star ($\lesssim 0.7''$) [NII] emission comes primarily from the high velocity jet implying this is the region with the highest excitation.
(vii) The medium velocity bow-shaped structure A1 is less evident in [SII] and [OI] than in Hα, suggesting that its excitation level may be high.
(viii) There is a strong low velocity peak in Hα emission coinciding with the star. This is almost certainly scattered emission from a region close to DG Tau, including possibly a magnetospheric contribution (Edwards 1997) and therefore does not constitute part of the outflow *per se*.

4. Discussion

The STIS observations presented here clearly show that the HVC emission in DG Tau comes from the most highly focused part of the outflow i.e. the jet. The jet at high velocities can be traced back to at least $0.1''$ (15 AU) from the star where quenching effects become important even in the case of the [OI]$\lambda\lambda$6300,6363 lines, which have the highest critical density ($\sim 10^6$ cm^{-3}) among the studied FELs. Obviously it is likely that the jet is collimated on even smaller scales. The shifts of the emission centroids in the different lines and in the different velocity bins can be explained quite naturally if there is an increase in jet density not only with proximity to the star (in the longitudinal direction) but also to the central outflow axis. That is to say the high velocity "core" of the jet is denser than its periphery. This is confirmed by an inspection of the [SII]$\lambda\lambda$6716,6731 doublet ratio (see Fig. 2 and Bacciotti et al. 2000). Note also that structures such as A1 and A2 are reminiscent of the "bubbles" recently seen by Krist et al. (1999) in the case of XZ Tauri. These

are almost certainly internal working surfaces caused by temporal variations in the outflow from DG Tau. Certainly there is plenty of evidence for strong jet velocity variations in DG Tau (and in many other CTTS stars) on timescales of years. For example, the data of Mundt et al. (1987) and Solf and Böhm (1993) show an increase in the radial velocity of the jet at D $\sim 0.5''$ by a factor of 2 within 8 years. Also the proper motion data of Eislöffel and Mundt (1998) indicate large velocity variations. Finally, several of the knots in the DG Tau jet show bow shock-like structures (see also the HST Archive data presented in Bacciotti et al. (2000)) and these provide indirect evidence for strong velocity variations.

Turning now to the LVC, its nature still remains somewhat enigmatic. It was already clear from groundbased observations that the LVC and HVC differ in many properties such as density and excitation. A new difference is reported here i.e. the rather large spatial width W of the LVC perpendicular to the jet at distances D of about $0.1''$–$0.3''$ from the source. A comparison of W (at FWHM) between the high and low-velocity emission in [SII] and [OI] shows that the average W(LVC) $\sim 0.18''$ while the HVC is hardly resolved at a distance D of $0.2''$. We note that this comparison of spatial widths can only be done using our [SII] and [OI] "images" as the Hα data is heavily contaminated by stellar Hα emission and in [NII] the LVC is very weak. Another interesting result of our study is the smaller velocity of the LVC at the edges of the flow (for full details see Bacciotti et al. (2000)). For example at D = $0.2''$ the LVC peaks at $\sim$ -95 km s^{-1} in [OI] for the central slit position (S4) while in the two outermost slit positions (S1,S7) it peaks at about -18 km s^{-1}. The corresponding values for the [SII] line are -60 km s^{-1} and -40 km s^{-1}, respectively. Since these lines are optically thin, such observations clearly point to a rise in the average LVC velocity as the central outflow axis is approached.

To what degree the observations of DG Tau presented here, particularly of the LVC, are representative of other CTTSs is an open question. DG Tau is one of the most active CTTSs known and we caution that the LVC of DG Tau is unusual in that it has the highest absolute velocity of all the CTTSs listed by Hartigan, Edwards, and Ghandour (1995), as well as one of the highest accretion rates. That said it shares the typical properties of other LVCs and, in particular, the ratio of its luminosity (L) to that of the DG Tau HVC is in perfect agreement with the L(HVC) v. L(LVC) relationship noted by Calvet (1997). Thus DG Tau may simply be displaying the higher activity tail of the distribution of outflow properties amongst CTTSs. In conclusion our STIS observations show, for the first time, a quasi-continuous variation in the outflow velocity close to a YSO in the transverse direction to the flow. Detailed studies are required, however, to test whether these observations can constrain models for the generation of the LVC and HVC.

We thank the anonymous referee for his/her very helpful comments. FB was supported by an European Space Agency contract at the Dublin Institute for Advanced Studies during the course of this work.

REFERENCES

Bacciotti, F., Ray, T.P., Mundt, R., Eislöffel, J., Solf, J. and Camenzind, M. 2000, in preparation

Calvet, N. 1997, in Herbig-Haro Flows and the Birth of Low Mass Stars, IAU Symp. 182, eds. B. Reipurth and C. Bertout (Kluwer Academic Publishers), 417

Camenzind, M. 1997, in Herbig-Haro Flows and the Birth of Low Mass Stars, IAU Symp. 182, eds. B. Reipurth and C. Bertout (Kluwer Academic Publishers), 241

Edwards, S. 1997, in Herbig-Haro Flows and the Birth of Low Mass Stars, IAU Symp. 182, eds. B. Reipurth and C. Bertout (Kluwer Academic Publishers), 433

Eislöffel, J., and Mundt, R. 1997, AJ, 114, 280

Eislöffel, J., and Mundt, R. 1998, AJ, 115, 1554

Hartigan, P., Edwards, S., and Ghandour, L. 1995, ApJ, 452, 736

Hartmann, L., and Raymond, J.C. 1989, ApJ, 337, 903

Hirth, G., Mundt, R., and Solf, J. 1994, A&A, 285, 929

Hirth, G., Mundt, R., and Solf, J. 1997, A&AS, 126, 437

Kepner, J., Hartigan, P., Yang, C., and Strom, S. 1993, ApJ, 415, 119

Kwan, J., and Tademaru, E., 1995, ApJ, 454, 382

Kwan, J., and Tademaru, E., 1998, ApJ, 332, 41

Krist, J.E., et al. 1999, ApJ, 515, 35

Lavalley, C., Cabrit, S., Dougados, C., Ferruit, P., and Bacon, R. 1997, A&A, 327, 671

Mundt, R., Brugel, E, and Bührke, T. 1997, ApJ, 319, 275

Mundt, R., and Fried, J., 1983, ApJ, 274, 83

Ouyed, R., and Pudritz, R.E. 1994, ApJ, 423, 753

Ray, T.P. 1996, in the NATO ASI on Solar and Astrophysical MHD Flows, ed. K. Tsinganos (Kluwer Academic Publishers), 539

Safier, P.N. 1993, ApJ, 408, 148

Solf, J. 1997, in Herbig-Haro Flows and the Birth of Low Mass Stars, IAU Sympos. 182, eds. B. Reipurth and C. Bertout (Kluwer Academic Publishers), 63

Solf, J., and Böhm, K.H. 1993, ApJ, 410, 31

Fig. 1.— Top panel: reconstructed Hα images of the optical outflow close to DG Tau in four distinct velocity bins: (from left to right) low from +59 to -67 $\mathrm{km\,s^{-1}}$, medium from -68 to -194 $\mathrm{km\,s^{-1}}$, high from -195 to -321 $\mathrm{km\,s^{-1}}$ and very high from -322 to -448 $\mathrm{km\,s^{-1}}$. In this, and Figs. 2 and 3, the flux density is displayed logarithmically from 10^{-16} to 10^{-12} $\mathrm{erg\,s^{-1}\,arcsec^{-2}\,cm^{-2}\,\AA^{-1}}$. The horizontal line marks the position of the star. The letters 'A1' and 'A2' mark two distinct structures in the flow, one of which, A1, is bow-like. Bottom panel: same as top panel, but for the [NII]λ6583 line. Velocity bins: +55 – -71 $\mathrm{km\,s^{-1}}$, -72 – -198 $\mathrm{km\,s^{-1}}$, -199 – -325 $\mathrm{km\,s^{-1}}$, and -326 – -452 $\mathrm{km\,s^{-1}}$.

Fig. 2.— Same as Fig. 1, but in the light of the [SII]λ6731 line (top panel) and [OI]λ6363 line (bottom panel). Velocity bins for the [SII] images: +52 – -71 $\mathrm{km\,s^{-1}}$, -72 – -195 $\mathrm{km\,s^{-1}}$, -196 – -319 $\mathrm{km\,s^{-1}}$, and -320 – -443 $\mathrm{km\,s^{-1}}$. The superposed numbers refer to the corresponding average electron density values in $\mathrm{cm^{-3}}$, calculated from the ratio of the [SII] lines. Velocity bins for the [OI] image: +73 – -57 $\mathrm{km\,s^{-1}}$, -58 – -188 $\mathrm{km\,s^{-1}}$, -189 – -319 $\mathrm{km\,s^{-1}}$, and -320 – -450 $\mathrm{km\,s^{-1}}$.

Fig. 3.— Same as Fig. 1, but only for the lowest velocities and in the light of the [SII]λ6731 line (top panel) and the [OI]λ6300 line (bottom panel). Velocity bins for both images are given in $\mathrm{km\,s^{-1}}$.

This preprint was prepared with the AAS LaTeX macros v5.0.

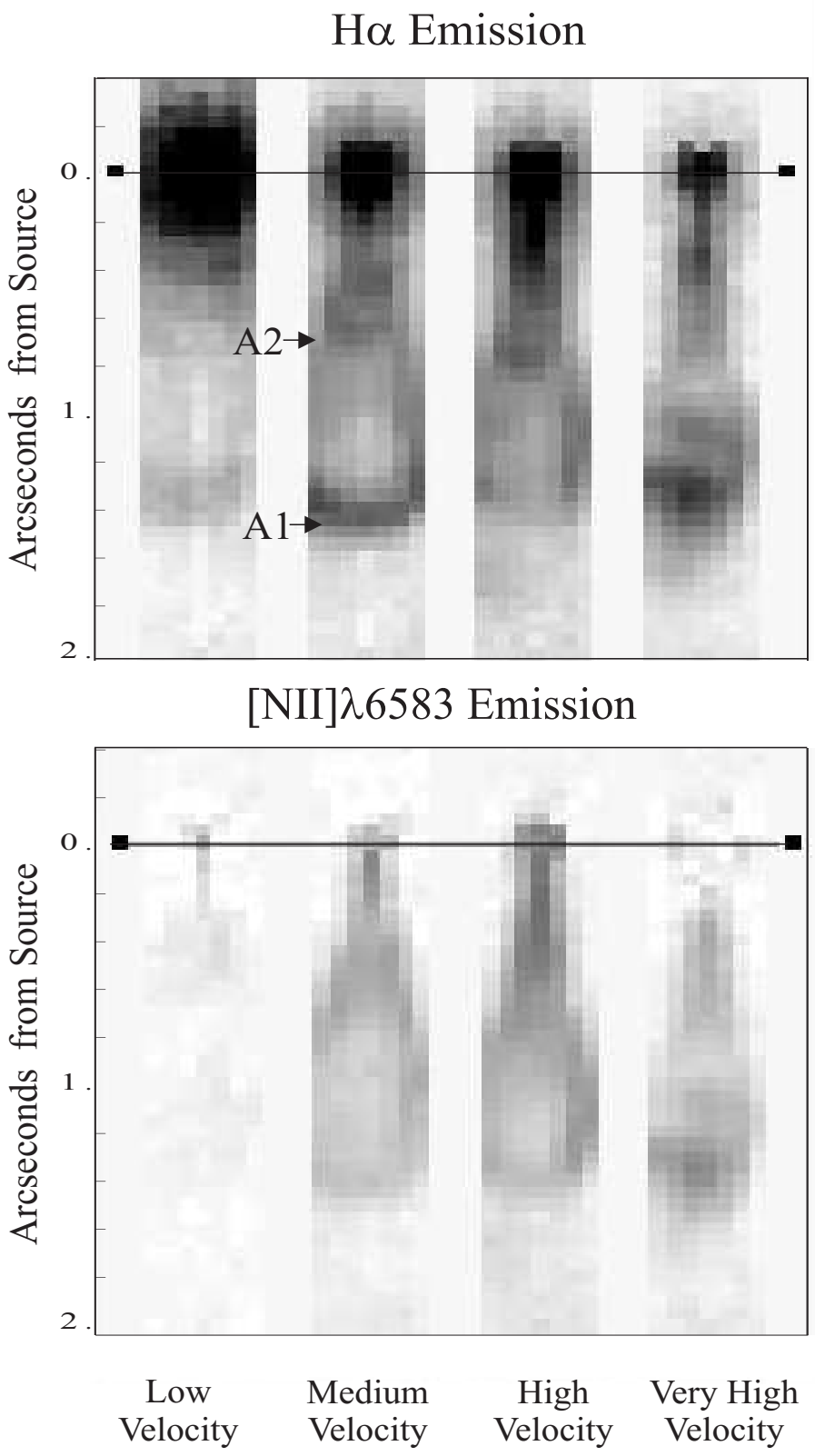
Hα Emission
Arcseconds from Source
0
1
2
A2
A1
[NII]λ6583 Emission
Arcseconds from Source
0
1
2
Low Velocity
Medium Velocity
High Velocity
Very High Velocity

Figure 1

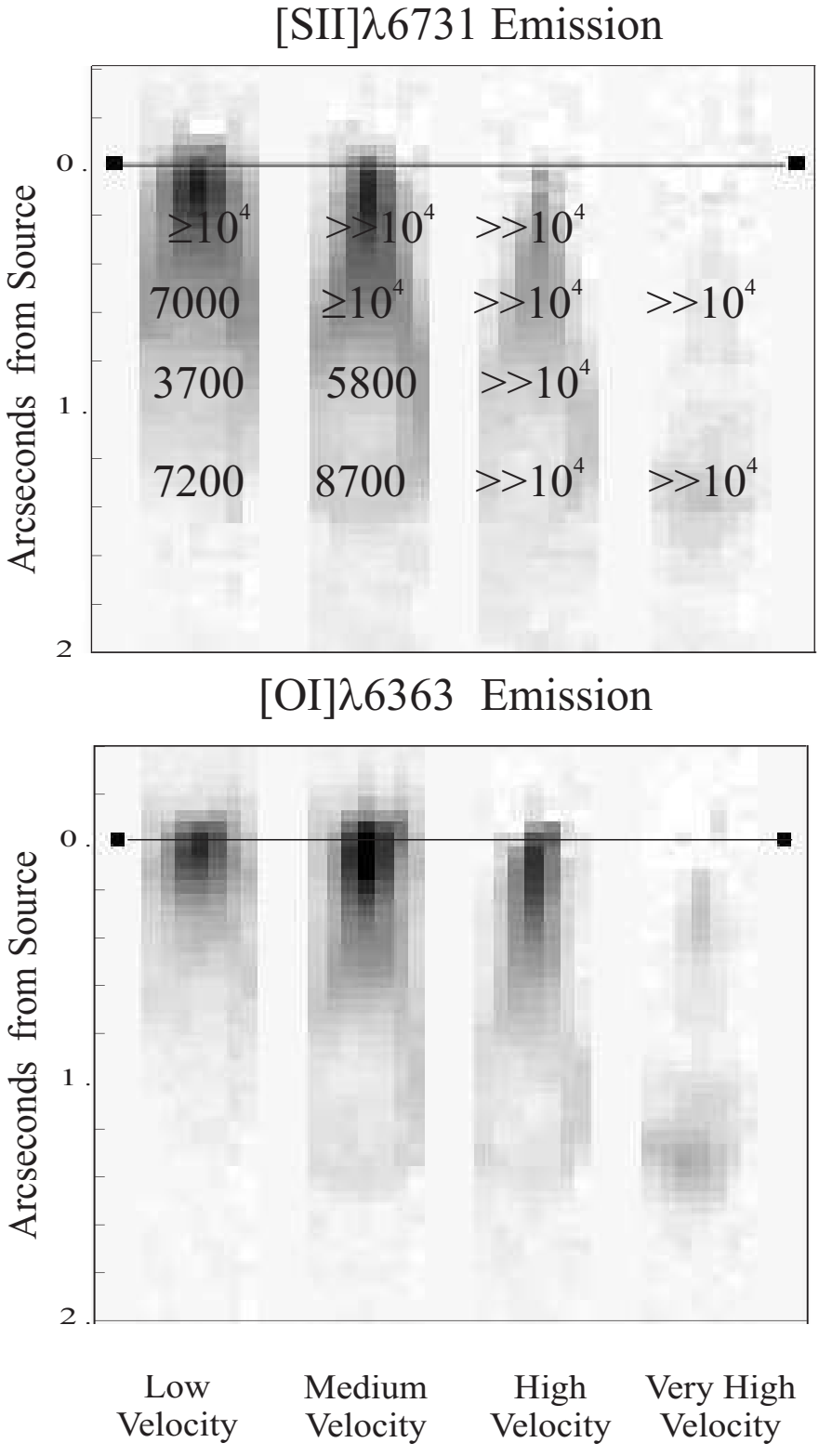
[SII]λ6731 Emission
Arcseconds from Source
0
1
2
≥10^4
>>10^4
>>10^4
7000
≥10^4
>>10^4
>>10^4
3700
5800
>>10^4
7200
8700
>>10^4
>>10^4
[OI]λ6363 Emission
Arcseconds from Source
0
1
2
Low Velocity
Medium Velocity
High Velocity
Very High Velocity

Figure 2

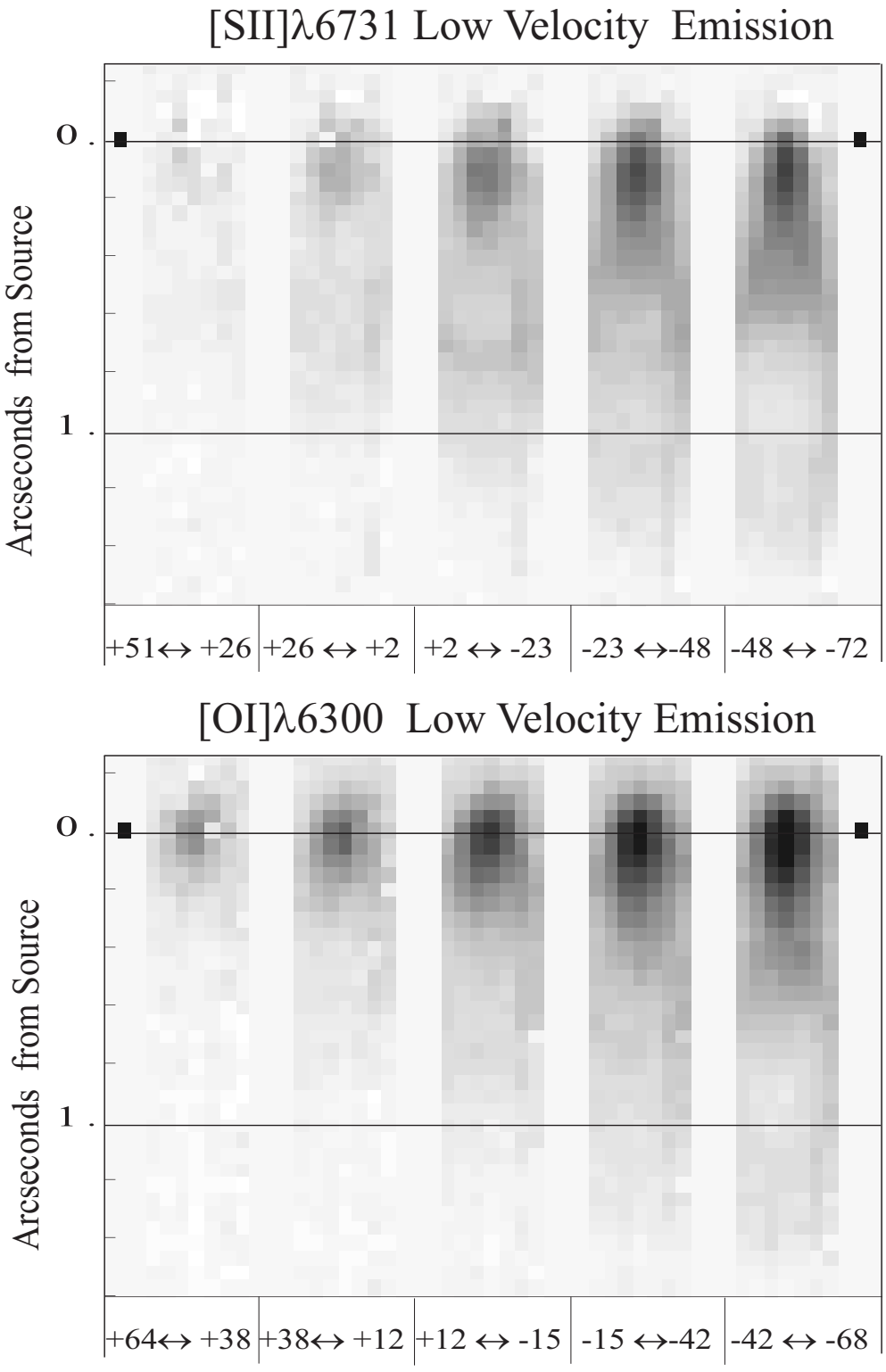
[SII]λ6731 Low Velocity Emission
Arcseconds from Source
0 .
1 .
+51↔ +26
+26 ↔ +2
+2 ↔ -23
-23 ↔-48
-48 ↔ -72
[OI]λ6300 Low Velocity Emission
Arcseconds from Source
0 .
1 .
+64↔ +38
+38↔ +12
+12 ↔ -15
-15 ↔-42
-42 ↔ -68

Figure 3